A Decomposition Method for MIMO OTA Performance Evaluation

Penghui Shen, *Student Member, IEEE*, Yihong Qi, *Senior Member, IEEE*, Wei Yu, *Member, IEEE*, Jun Fan, *Fellow, IEEE*, Zhiping Yang, *Senior Member, IEEE*, and Songping Wu, *Member, IEEE*

***Abstract*—Diagnosis and troubleshooting are critical to efficiently detecting the imperfections and improving the radio frequency designs for wireless systems in the research and development stage. For achieving these, this paper proposes a decomposition method for the measurement of multi-input multi-output (MIMO) devices' over-the-air (OTA) performance. By using the proposed method, the antenna active envelope correlation coefficient, the radiated sensitivity of each receiver, the total isotropic sensitivity, the self-interference, and the desensitization can all be achieved separately, and in the OTA working mode. In consideration of the MIMO system's complex array antennas and radio frequency receivers, the parameters obtained by this decomposition method are significant for discovering the imperfections, for debugging, and for improving the design of the devices. It is a valuable tool to raise the debugging efficiency of MIMO systems.**

***Index Terms*—Decomposition method, multi-input multi-output (MIMO), diagnosis, over-the-air (OTA).**

I. Introduction

WHAT is the chief concern of engineers if their multi-input and multi-output (MIMO) wireless systems fail to pass the network measurements? Detecting the imperfections and improving the radio frequency (RF) designs. The MIMO technique is the basis of 4G and coming 5G wireless communications because of its high data rates and better quality of signals. Currently, according to the international standard white papers [1], [2], the only figure of merit to evaluate MIMO devices' integrated over-the-air (OTA) performance is throughput; that is also the only criterion for OTA network measurement to separate the good and bad MIMO devices [3], [4]. For manufacturers and research and development (R&D) operators, one primary problem remains: how to detect imperfections and improve RF designs for bad devices.

The current standard methods for MIMO OTA measurement are not able to meet the technical requirements for troubleshooting MIMO devices under test (DUTs), as we shall see below. Multi-streams of data are transferred simultaneously in MIMO communication, which takes advantage of the spatial diversity in fading channels [5]–[7]. As a result, the fading channel characteristics are an integral part of the test conditions and directly influence the DUT's MIMO OTA performance [8]–[14]. MIMO OTA measurements should be carried out based on channel models which accurately reflect the standard wireless propagation environment (accounting for all the relevant aspects such as angles of departure, angles of arrival, angle spreads, cross-polarization rate, etc.) [15].

The Third Generation Partnership Project (3GPP) [16] and the Cellular Telecommunication and Internet Association (CTIA) [17] have presented many MIMO OTA measurement white papers for standardizations of MIMO OTA measurement [2], [11], [18]. At the end, only two methods were approved: the multi-probe anechoic chamber (MPAC) method [2], and the radiated two-stage (RTS) method [1]. The multi-path environment is realized through a channel emulator plus multiple probes in the MPAC method, which requires at least 16 probes for a 2D channel model realization [2]. The RTS method is based on the fact that the received signals at the MIMO receivers can be simulated by instruments integrating the measured antenna patterns and the channel models, and then fed into the receivers OTA [1], [19], [20].

The two methods are the same in theory foundation, but different in realizations. In MPAC, a large number of probes is needed to surround the DUT to simulate the multi-path channel. This complex hardware set-up brings in numerous test uncertainties and difficulties for calibrations. By contrast, the RTS method is based on a first stage of MIMO device antenna patterns measurement, and followed by a second stage of combining the measured patterns with channel fading for the throughput test. The RTS method is a more cost-efficient solution, since just a single-input single-output (SISO) chamber is required to do the MIMO OTA measurements [21], [22].

With those two techniques, the throughput result is accurately measured. However, this result is not sufficient for an accurate and reliable product debugging and RF design improvement. MIMO terminals have a complex RF system, which includes

Manuscript received September 14, 2017; revised January 25, 2018 and April 2, 2018; accepted May 20, 2018. Date of publication May 23, 2018; date of current version September 17, 2018. This work was supported in part by the Chinese Ministry of Education–China Mobile Research Foundation under Grant MCM 20150101 and in part by the National Natural Science Foundation of China under Grant 61671203. The review of this paper was coordinated by Prof. J. Liu. *(Corresponding author: Yihong Qi.)*

P. Shen is with Hunan University, Changsha 410082, China and also with General Test Systems Inc., Shenzhen 518000, China (e-mail: 1148115376@qq.com).

Y. Qi is with Hunan University, Changsha 410006, China with General Test Systems Inc., Shenzhen 518102, China, and also with the Missouri University of Science and Technology, Rolla, MO 65409 USA (e-mail: yihong.qi@generaltest.com).

W. Yu is with General Test Systems Inc., Shenzhen 518000, China (e-mail: fred.yu@generaltest.com).

J. Fan is with the Missouri University of Science and Technology, Rolla, MO 65409 USA (e-mail: jfan@mst.edu).

Z. Yang and S. Wu are with Google, Mountain View, CA 94043 USA (e-mail: zhipingyang@google.com; songpingwu@google.com).

Color versions of one or more of the figures in this paper are available online at http://ieeexplore.ieee.org.

Digital Object Identifier 10.1109/TVT.2018.2839726

array antennas, multi-receivers, and RF circuits for beam forming. The integrated MIMO wireless performance (including the throughput result) is determined by many factors such as number of antennas, antenna envelope correlation coefficient (ECC), receiver radiated sensitivity, noise, desensitization (also called "desense" for short), and self-electromagnetic interferences (EMI) [23]–[26]. Throughput measurement is significant to separate the good and bad MIMO devices, but almost useless to tell engineers which exact modules in the bad products need to be improved.

In order to solve this issue, a decomposation measurement method for MIMO system diagnosis was developed. In this way, the muti-antennas' ECC, the receivers' radiated sensitivities, the total isotropic sensitivity (TIS), the received noise levels, and the sensitivity desensitization caused by any other module are all obtained for DUT diagnosis. The method is significant for R&D based on the following reasons:

1) As is widely recognized, the DUT integrated OTA performance differs from the conducted antenna performance plus the conducted receiver performance [11], [27], [28]. Moreover, the antennas and receivers are in general designed by different engineers or departments. By using the proposed method, the MIMO device antennas, the RF receivers and the noise are measured separately, in the device's real working mode (without intrusive cables). From the results, engineers could clearly discover the imperfect parts, which is helpful to improve their designs. In summary, the decomposation method is also useful to raise the work efficiency.
2) According to the CTIA test plan [11], the radiated sensitivity is one of the most important criterion to evaluate the receiver's receiving capability, which may be greatly affect by the noise (mainly caused by the antennas, the ciucuits, the temprature, etc.). It is the first time that the radiated sensitivities of all receivers are measured separately for a MIMO DUT in OTA working mode.
3) The noise level evaluations is very important for the MIMO DUT EMI analysis. Further, conducting the noise measurements in different modes (for example: with WiFi circuit on and off), the obtained results are helpful to troubleshoot the self-interference.
4) Different from the conducted method where the interference and noise radiated by the user equipment (UE) cannot be considered, all the proposed measurements are conducted OTA, in the conditions of multiple receivers' coexistence, allowing the results to highly reflect the performances of all parts in their actual working conditions [27].

Especially for 5G massive MIMO system, the array antennas and the RF receivers are usually integrated on-chip; no RF connections are reserved for debugging. Measurements for every RF module OTA are urgently required. Therefore, the decomposition test method is a valuable tool for MIMO R&D.

The remainder of this paper is arranged as follows. Section II discusses the foundation theory of the decomposition measurement method. The test configrations and procedure are introduced in Section III, followed by the experiments and analysis in Section IV. And finally, the conclusions are proposed in Section V.

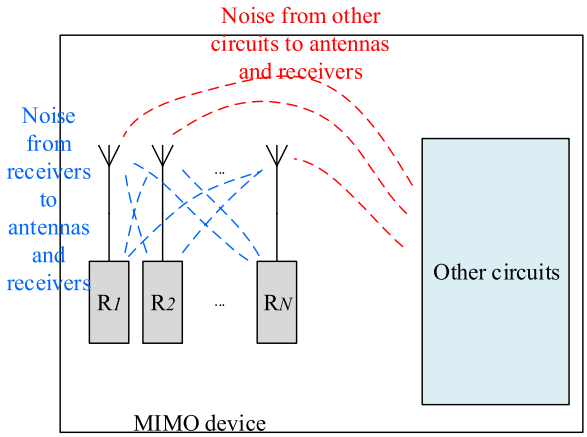

Fig. 1. A typical N × N MIMO system simplified diagram includes three parts required to be measure: the antenna system, the RF receivers, and the self-desensitization.

II. The Foundation Theory of the Decomposition Measurement Method

The decomposition method is based on the following two parts: *A*) equipment decompositions and *B*) theory of the decomposition measurement.

A. Equipment Decompositions

A typical N × N MIMO system is sketched in Fig. 1. Both the communication signals and the noise (mainly caused by the DUT circuits and the device temperature distribution) could be coupled through the antennas and fed into the RF receivers. To clearly debug the MIMO DUT, three parts are measured separately by using the proposed method: the antenna system, the receiver system, and the self-interferences.

1) Antenna System: The active antenna ECC is measured for the multiple antennas' coupling evaluations. MIMO takes advantage of antenna diversity techniques to increase spectrum efficiency; however, mutual coupling of the multi-antenna system degrades the performance. The factor ECC is just used to evaluate the antenna system's cross-coupling, which is expressed as:

$$ECC = \frac{\left|S_{11}^{*} \times S_{12} + S_{21}^{*} \times S_{22}\right|^{2}}{\left(1 - \left(\left|S_{11}\right|^{2} + \left|S_{21}\right|^{2}\right)\right)\left(1 - \left(\left|S_{22}\right|^{2} + \left|S_{12}\right|^{2}\right)\right)}, \tag{1}$$

where S_{xy} are the S-parameters, and $*$ denotes the conjugate transformation. It is worth mentioning that in the proposed method, the S-parameters are achieved in the radiated test mode. Thus, the antenna ECC, a number between 0 and 1, is calculated. The larger the number, the higher the correlation it indicates.

2) The Receiver System: For the receiver system diagnosis, the radiated sensitivity and the TIS values are measured. As presented in the CTIA test standard [11], radiated sensitivity is the special downlink power at the RF receiver input (antenna's output), which meets the air-link's minimum performance criterion (typically indicated by bit, block, or frame error rate). Taking the Global System for Mobile Communication (GSM) protocol for example, the power at the UE receiver input, which

makes the UE operate at 2.44% bit error rate (BER), is the corresponding radiated sensitivity.

It is recognized that the radiated sensitivity differs from that measured in a conducted test mode due to self-desensitization and other non-linear behaviors. Additionally, the radiated sensitivity can reflect the true working performance of the receiver. In the proposed approach, all the radiated sensitivities are measured.

According to the measured radiated sensitivities and the antenna patterns (the antenna patterns could be obtained in the mentioned RTS measurement method for MIMO OTA evaluations), the TIS values can be calculated.

TIS is one basic metric for single air-link wireless performance evaluation (a single air-link includes an antenna and its corresponding receiver). Further, TIS is used to evaluate the UE's receiving capacity for weak signals. Based on the CTIA test standard [11], TIS is computed by integrating the efficient isotropic sensitivity (EIS) over a 3D surface as

$$\text{TIS\_value} = \frac{1}{\frac{1}{4\pi} \times \oint \left[\frac{1}{EIS_{x,DUT}(\theta,\phi)}\right] \sin(\theta)\, d\theta d\phi}. \quad (2)$$

Alternatively, EIS is defined as

$$\text{EIS}_{x,DUT}(\theta,\phi) = \frac{P_{rs}}{\text{G}_{x,DUT}(\theta,\phi)}, \quad (3)$$

where P_{rs} is the stated radiated sensitivity, which is an angle-independent factor, and $\text{G}_{x,DUT}(\theta,\phi)$ is the corresponding antenna gain in polarization x and at angle (θ,ϕ).

Moreover, the TIS imbalance between any two air-links is calculated.

3) Self-Interference: For the self-interference estimations, the noise levels at the receiver input ports are measured to discover the desensitization. In the tightly coupled MIMO system, the noise generated by its own system would couple back to the antenna and contribute to the noise level of the receiving system, as shown in Fig. 1. The noise may cause significant sensitivity degradations. Thus the noise test is fundamental for solving the desensitization issues.

For simplification, we will take the GSM protocol as an example in this part to explain the desensitization issues. For a fixed RF receiver, the radiated sensitivity is determined by the signal noise rate (SNR) value at the receiver input with its correspondence antenna attached. Following [25], the relationship between BER and the SNR value is presented as

$$\text{BER} = \frac{1}{2} erfc\left(\sqrt{\frac{SNR}{f_{bit}}}\right), \quad (4)$$

where *SNR* is the SNR value of the received signal at the receiver input port, and f_{bit} is the bit rate which is considered as a constant under an unchanged frequency and protocol mode [25], [26].

As shown in Fig. 1, the blocks including the RF circuits, the digital modules and the power sources are all the noise sources existed and required to be measured in the DUT. In this paper, the noise contributors are all evaluated separately, which is meaningful for the EMI analysis for the MIMO UE.

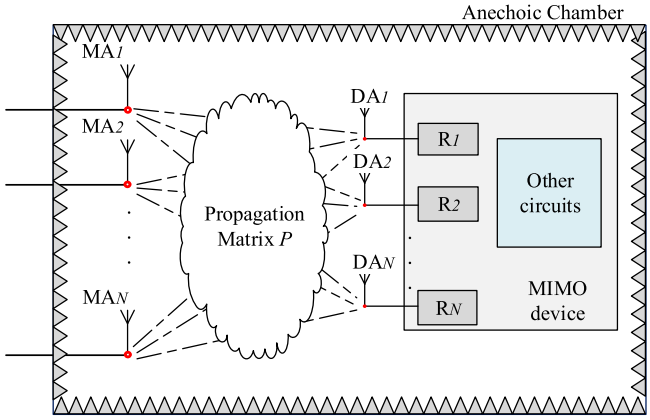

Fig. 2. The propagation matrix *P* is the description for the signal offsets (including the power path loss and phase offset) between the reference antenna feedings in chamber and the RF receiver inputs in MIMO device.

B. Theory of the Decomposition Measurement

In Fig. 2, the MIMO device is located in an anechoic chamber, where MA is the measurement antenna in the chamber, DA is the MIMO antenna in the actual DUT. The electromagnetic wave from any measurement antenna could be coupled into all the DA and then fed into the receivers. This coupling situation is described as a propagation matrix *P*:

$$\text{P} = \begin{bmatrix} p_{11} & p_{12} & \cdots & p_{1N} \\ p_{21} & p_{22} & \cdots & p_{2N} \\ \vdots & \vdots & \ddots & \vdots \\ p_{N1} & p_{N2} & \cdots & p_{NN} \end{bmatrix}, \quad (5)$$

where p_{xy} is vector offset from the *y*-th measurement antenna feeding to the *x*-th receiver input. The propagation matrix *P* is relative to the information about the propagation path loss in chamber, the gains of the chamber antennas and the DUT antennas, and the phase offsets between the DUT receivers and the reference antenna feedings.

Then the relationship between the feeding vectors at measurement antennas (marked as $NT_1, NT_2, \ldots, NT_N$) and the received signals at receiver inputs (marked as $BR_1, BR_2, \ldots, BR_N$) is

$$\begin{bmatrix} BR_1 \\ BR_2 \\ \vdots \\ BR_N \end{bmatrix} = \begin{bmatrix} p_{11} & p_{12} & \cdots & p_{1N} \\ p_{21} & p_{22} & \cdots & p_{2N} \\ \vdots & \vdots & \ddots & \vdots \\ p_{N1} & p_{N2} & \cdots & p_{NN} \end{bmatrix} \times \begin{bmatrix} NT_1 \\ NT_2 \\ \vdots \\ NT_N \end{bmatrix}. \quad (6)$$

Equation (6) is the basis of the decomposition measurement method. Taking the first receiver's radiated sensitivity measurement for example, the received signals at all other receiver inputs should be zero, as

$$\begin{bmatrix} 1 \\ 0 \\ \vdots \\ 0 \end{bmatrix} = \begin{bmatrix} p_{11} & p_{12} & \cdots & p_{1N} \\ p_{21} & p_{22} & \cdots & p_{2N} \\ \vdots & \vdots & \ddots & \vdots \\ p_{N1} & p_{N2} & \cdots & p_{NN} \end{bmatrix} \times \begin{bmatrix} NT_1 \\ NT_2 \\ \vdots \\ NT_N \end{bmatrix}. \quad (7)$$

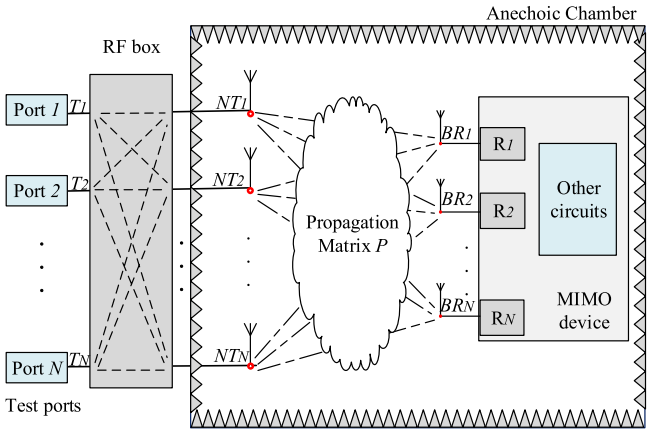

Fig. 3. An N × N RF box is configured between the test instrument output ports and the measurement antenna feedings.

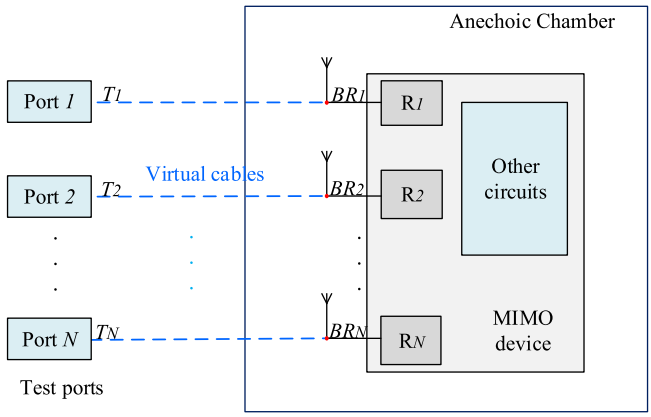

Fig. 4. Simplified schematic diagram for Fig. 3.

With the propagation matrix and the desired received signals known, the signals required to be fed into the measurement antennas (NT_1, NT_2, …, NT_N) are calculated. Then, the radiated sensitivity for the first receiver is measured (the detailed test procedure will be described in the rest).

Moreover, an N × N RF circuit is configured between the test ports and the measurement antenna feedings, as shown in Fig. 3. The S-parameters of the RF circuit are marked as matrix *B* in the paper. Then, the relationship between the test ports output signals (marked as T_1, T_2, …, T_N) and the received signals at receivers is

$$\begin{bmatrix} BR_1 \\ BR_2 \\ \vdots \\ BR_N \end{bmatrix} = \begin{bmatrix} p_{11} & p_{12} & \cdots & p_{1N} \\ p_{21} & p_{22} & \cdots & p_{2N} \\ \vdots & \vdots & \ddots & \vdots \\ p_{N1} & p_{N2} & \cdots & p_{NN} \end{bmatrix} \times \begin{bmatrix} b_{11} & b_{12} & \cdots & b_{1N} \\ b_{21} & b_{22} & \cdots & b_{2N} \\ \vdots & \vdots & \ddots & \vdots \\ b_{N1} & b_{N2} & \cdots & b_{NN} \end{bmatrix} \times \begin{bmatrix} T_1 \\ T_2 \\ \vdots \\ T_N \end{bmatrix}, \tag{8}$$

where b_{xy} is an S-parameter of the RF box.

If the S-parameters matrix representing the RF circuit is set to be the inverse of the propagation matrix *P*, then we have

$$\begin{bmatrix} BR_1 \\ BR_2 \\ \vdots \\ BR_N \end{bmatrix} = \begin{bmatrix} T_1 \\ T_2 \\ \vdots \\ T_N \end{bmatrix}. \tag{9}$$

Equation (9) indicates that the signal BR_x at the *x*-th receiver only sources from the *x*-th test port, without crosstalk.

Based on (9), the test ports can reach the receiver inputs directly, similar to the conducted mode. So Fig. 3 is further simplified as Fig. 4, where virtual cables are defined as virtual connections between the test ports and receiver inputs. Compared with the real cable connections, the virtual cables have several advantages.

1) The virtual connections do not change the matching inside the DUT.
2) The noise contributed by the DUT or the environment are still considered.
3) The virtual cable conducted way is a non-intrusive measurement solution.

Therefore, based on the virtual cable concept, the RF receivers can be reached and then measured separately. The detailed test procedure and calculations are provided as below.

III. The Measurement Procedure and Result Calculations of the Decomposition Method

A. Measurement Process

The decomposition test system is illustrated in Fig. 3. The test procedure is divided into the following steps:

1) Fix the DUT in a chamber with at least *N* measurement antennas inside.
2) Set the N × N RF S-parameter matrix equal to the inverse of the propagation matrix.
3) With a two-port vector network analyzer (VNA) connected to the RF box test ports, measure the S-parameters between any two DUT antenna feedings. The factors are obtained without RF cables, so the antenna active ECC is calculated out through (1).
4) With a base station emulator (BSE) connected to the RF box test ports, measure the radiated sensitivities of all the receivers seperately. The detailed measurement process for the *x*-th receiver radiated sensitivity is introduced as follows:
   a) Connect the BSE output to the RF box's *x*-th test port and keep the vectors at the other test ports zero.
   b) Adjust the BSE output power step by step until reaching the threshold BER (2.44%, for example, in the rest of the paper).
   c) Record the downlink power as the radiated sensitivity of the *x*-th receiver (marked as P_{rs_x}).
5) Compared with the set-up in step 4, a non-loss additive white Gaussian noise (AWGN) source is added to the RF box test ports. The radiated sensitivities of all the receivers are measured in the SNR test mode in this step. The measurement set-up is illustrated in Fig. 5, where the BSE

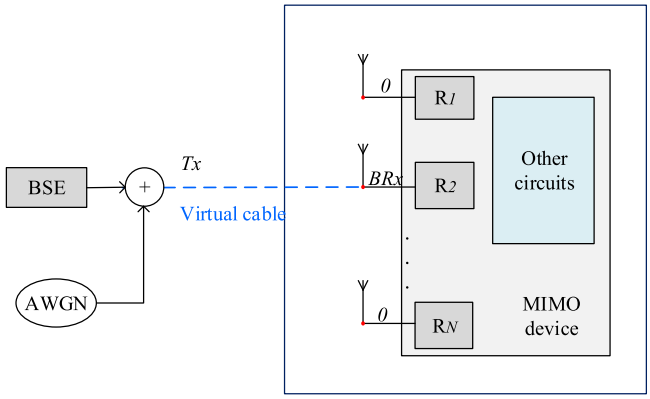

Fig. 5. With the AWGN source applied, the radiated sensitivity is measured in the SNR mode.

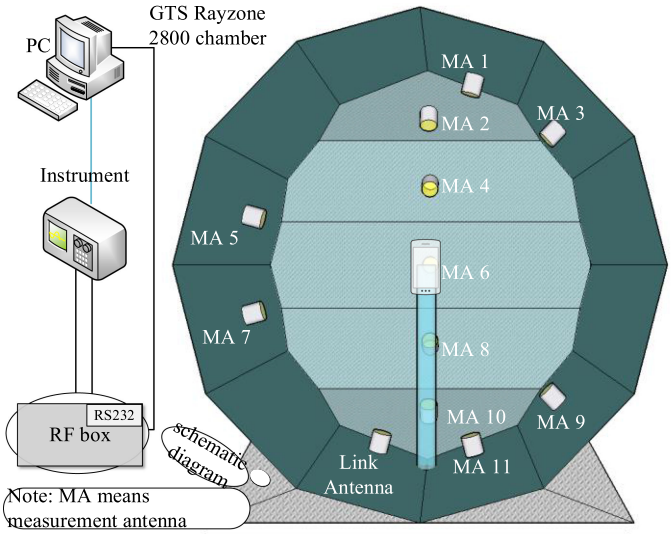

Fig. 6. Validation test system for decomposition measurement.

TABLE I
TEST MEASUREMENT PARAMETERS

Parameters	Value
Instrument	Keysight UXM
Anechoic chamber	RayZone 2800 from GTS
Downlink frequency	2132.5 MHz
Protocol	FDD
DUT	Samsung Tab2
Channel model	SCME UMi

output communication signal and the AWGN are combined and then fed into the receiver directly. The detailed measurement process for the x-th receiver is introduced as follows:

a) The DUT should be in the same configurations as in step 4.
b) Connect the BSE and the AWGN source as in Fig. 5 and keep the vectors at the other test ports zero.
c) Turn on the BSE and turn off the AWGN source.
d) Keep the BSE output power level of signal T_x fixed (which is much larger than P_{rs_x} recorded in step 4 as P_{nrs_x}).
e) Turn on the AWGN source. Adjust the AWGN noise level step by step until the x-th receiver works at its threshold BER (2.44%).
f) Record the noise level (the AWGN source output) as N_{snr_x}.

It should be noted that in step 4, the downlink power of the BSE is adjusted step by step until reaching the threshold BER. In step 5, the downlink power of the BSE is kept fixed and the noise level is adjusted step by step until reaching the threshold BER; this is referred to as the "SNR test mode".

B. Results Calculations

The ECC values and the radiated sensitivities are directly read from the instruments in steps 3 and 4. With known antenna gains, the TIS values are computed by using (2) and (3).

Equation (4) indicates that with unchanged frequencey and modulations, a fixed BER value corresponds to one, and only one, constant SNR. Assuming in step 4 the noise level at the x-th receiver, named as N_{nor_x}, is mainly caused by the DUT itself, then for the x-th receiver, the radiated sensitivity is related to the noise as:

$$2.44\% = \frac{1}{2} erfc\left(\sqrt{\frac{P_{rs\_x}}{N_{nor\_x}} \times \frac{1}{f_{bit}}}\right). \tag{10}$$

Further in step 5, the SNR value which ensures the x-th receiver operating at the 2.44% BER, was achieved. The noise level at the x-th receiver includes two parts: the self-interference N_{nor_x} (since the DUT configurations in the step 4 and 5 are the same, the self-interference is unchanged) and the artificially added noise due to the instrument (marked as N_{snr_x}). The BER value is related to the SNR as,

$$2.44\% = \frac{1}{2} erfc\left(\sqrt{\frac{P_{nrs\_x}}{N_{nor\_x} + N_{snr\_x}} \times \frac{1}{f_{bit}}}\right). \tag{11}$$

Since the *erfc* function is strictly monotone, based on (10) and (11), it is clear that

$$\frac{P_{rs\_x}}{N_{nor\_x}} = \frac{P_{nrs\_x}}{N_{nor\_x} + N_{snr\_x}}. \tag{12}$$

Rewriting (12), we have

$$(P_{nrs\_x} - P_{rs\_x}) \times N_{nor\_x} = P_{rs\_x} \times N_{snr\_x}. \tag{13}$$

Since P_{nrs_x} is much larger than P_{rs_x}, (13) becomes

$$\frac{P_{rs\_x}}{N_{nor\_x}} = \frac{P_{nrs\_x}}{N_{snr\_x}}, \tag{14}$$

where P_{nrs_x}, P_{rs_x} and N_{snr_x} are all known from the instruments, so the noise level N_{nor_x} can be evaluated. Therfore, in this part, the noise levels at the receivers' input ports are measured, which may significantly affect the MIMO DUT OTA performance.

This noise measurement technique can be also wisely used in the DUT EMI analysis by repeating steps 4 and 5 in different DUT working modes (i.e., with the display on and off). The measured radiated sensitivities and noise levels clearly reflect the desensitization effects caused by the EMI stemming from the display block.

TABLE II
MEASUREMENT RESULTS

Parameters			Baseline Results				Difference		
			Baseline	Display On	Front camera on	Rear Camera on	Display On	Front camera on	Rear camera on
LTE B4	Total	Throughput @ 70% max	-99.75 dBm	-99.04 dBm	-94.95 dBm	-92.93 dBm	-0.71 dB	-4.80 dB	-6.82 dB
	Antennas	ECC	0.013						
		Antenna gain 1	-4.72 dB						
		Antenna gain 2	-5.50 dB						
		Gain imbalance	0.78 dB						
	RF receivers	Radiated sensitivity 1	-99.05 dBm	-98.27 dBm	-92.02 dBm	-89.12 dBm	-0.78 dB	-7.03 dB	-9.93 dB
		Radiated sensitivity 2	-97.21 dBm	-96.49 dBm	-94.41 dBm	-94.78 dBm	-0.72 dB	-2.80 dB	-2.43 dB
		TIS value 1	-94.33 dBm	-93.55 dBm	-87.30 dBm	-84.40 dBm	-0.78 dB	-7.03 dB	-9.93 dB
		TIS value 2	-91.71 dBm	-90.99 dBm	-88.91 dBm	-89.28 dBm	-0.72 dB	-2.80 dB	-2.43 dB
	Noise	Noise level 1	-99.55 dBm	-98.88 dBm	-92.72 dBm	-89.75 dBm	-0.67 dB	-6.83 dB	-9.80 dB
		Noise level 2	-97.72 dBm	-97.10 dBm	-94.88 dBm	-95.35 dBm	-0.62 dB	-2.84 dB	-2.37 dB

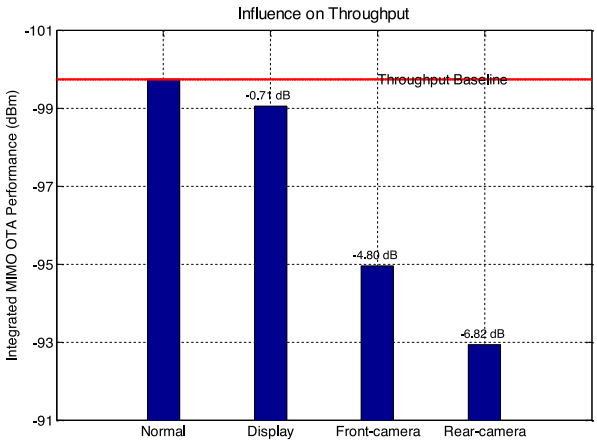

Fig. 7. The integrated influence on throughput contributed by the DUT inter noise.

IV. VALIDATIONS AND ANALYSIS

A 2×2 MIMO device was measured for validation of the proposed approach. In order to clearly show how the noise does influence the radiated sensitivity and the final throughput of the devices, several experiments were conducted with the DUT's inter-circuits on and off, including the display, the front camera, and the rear camera (i.e., the three blocks are used as electromagnetic interference sources). Further, for the DUT MIMO throughput performance evaluations, the standard RTS method is used.

The detailed test procedure is as follows:

1) Keep all the three noise sources off and conduct the following baseline measurement steps.
   a) Measure the throughput result by using the RTS MIMO OTA test method;
   b) Carry out the decomposition measurement for diagnosis by using the proposed method in this paper.
2) Keep the display on (the other two blocks off) and repeat the above two measurement steps. The results are used to reflect the desensitization caused by the display circuit.
3) Only keep the front camera on and repeat the measurement.
4) Only keep the rear camera on and repeat the measurement.

From the throughput comparisons, the global impact due to the three sources is clearly shown. Then, from the decomposition comparisons, the explanations for the uncertainties contributed by every source are clearly detailed.

A. Test Settings

The test configurations for the decomposition MIMO OTA measurement method is illustrated in Fig. 6, containing a control PC, MIMO measurement instruments (including a VNA and a BSE), an anechoic chamber with multiple reference antennas (GTS RayZone 2800 [29]), an RF box for 2×2 matrix settings, and a 2×2 MIMO terminal.

The test parameters are in Table I. It is worth noting the following several points:

1) The Spatial Channel Model Extension (SCME) Umi (detailed in the 3GPP technical report [1]) was conducted for final throughput tests.
2) The recorded downlink power results in the receiver working at the 4.00% BER value for the 4G Long Term Evolution (LTE) protocol, as the measured radiated sensitivity.
3) All the results in this section are in dB units.

B. Results and Analysis

The measurement results are shown in Table II; from them several conclusions can be drawn.

1) The display block has little influence on the integrated MIMO OTA performance. However, both cameras have great impact on DUT throughput (>4.8 dB), as shown in Fig. 7, where the *x*-axis lists the noise source and the *y*-axis shows the magnitudes of throughput performance.
2) The two active antenna efficiency factors are -4.72 dB and -5.50 dB, respectively. The ECC between the two antennas is very low (0.013).
3) The radiated sensitivity degradations caused by the three noise sources are shown in Fig. 8. It is clear that both the cameras have greater impact on the first receiver.
4) The noise levels are changed under different working statements. The measured values are useful for the EMI analysis and antenna temperature evaluations, which is detailed in [27].

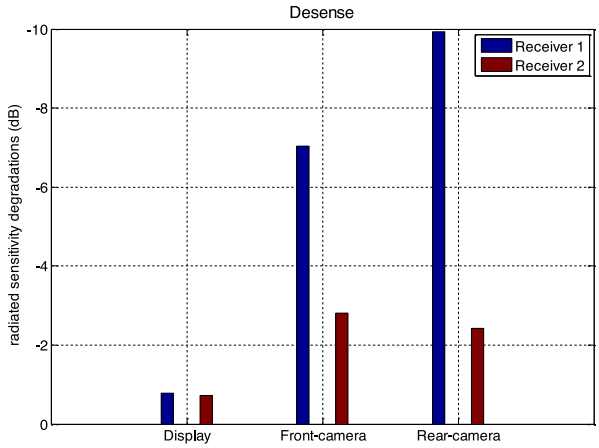

Fig. 8. The desensitization at different receivers.

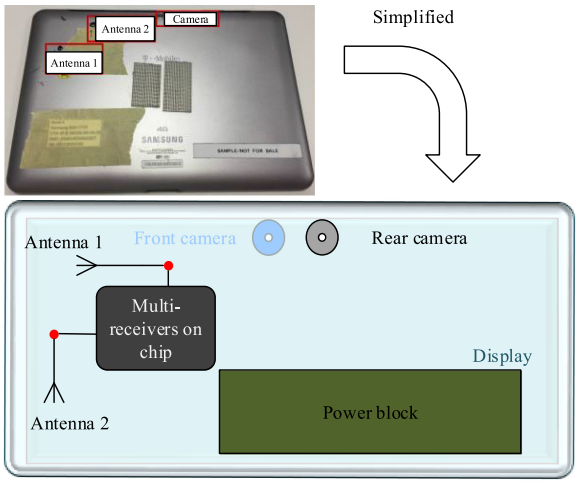

Fig. 9. The DUT and its simplified diagram.

The DUT is shown and simplified in Fig. 9. From the DUT physical design, it is natural to come to the following two considerations: the distance between the two antennas is very close to half wavelength at 2.1325 GHz (7 cm); therefore, the correlation between the two antennas is small. And the camera circuits could cause larger radiated sensitivity degradations for receiver 1 than receiver 2. From Fig. 9, it is also evident that the two cameras are much farther from the feeding point of antenna 1 than from the feeding point of antenna 2.

V. Conclusion

A decomposition MIMO OTA test method for MIMO terminals is proposed in this contribution. By using the proposed method, the ECC, the radiated sensitivity, the TIS, and the self-interference are all measured separately. All the measurements are carried out in the radiated working mode, without intrusive connections and in the conditions of multiple receivers' coexistence. Thus, the results can highly reflect the performances of each part in their normal working conditions.

Further, experiments were conducted on a 2×2 MIMO device to show how to use the decomposition parameters for a better engineering of the MIMO device, which also indicates that the decomposition can discover significant noise sources that cannot be diagnosed by any other means. The decomposition shows the presented technique is a useful tool for design troubleshooting in the initial stage of product development.

References

[1] 3GPP Technical Report 37.977 v12.0.0, 2017. [Online]. Available: http://www.3gpp.org
[2] *Test Plan for 2x2 Downlink MIMO and Transmit Diversity Over-the-Air Performance, Revision 1.1*, CTIA, Washington, DC, USA, Aug. 2016.
[3] X. Zhang, X. Shen, and L. Xie, "Uplink achievable rate and power allocation in cooperative LTE-advanced networks," *IEEE Trans. Veh. Technol.*, vol. 65, no. 4, pp. 2196–2207, Apr. 2016.
[4] Y. Jing, Z. Wen, H. Kong, S. Duffy, and M. Rumney, "Two-stage over the air (OTA) test method for MIMO device performance evaluation," in *Proc. IEEE Int. Symp. Antennas Propag.*, 2011, pp. 71–74.
[5] W. Yu, Y. Qi, K. Liu, Y. Xu, and J. Fan, "Radiated two-stage method for LTE MIMO user," *IEEE Trans. Electromagn. Compat.*, vol. 56, no. 6, pp. 1691–1696, Dec. 2014.
[6] J. Liu and W. Sun, "Smart attacks against intelligent wearables in people-centric internet of things," *IEEE Commun. Mag.*, vol. 54, no. 12, pp. 44–49, Dec. 2016.
[7] J. Liu, H. Nishiyama, N. Kato, and J. Guo, "On the outage probability of device-to-device communication enabled multi-channel cellular networks: A RSS threshold-based perspective," *IEEE J. Sel. Areas Commun.*, vol. 34, no. 1, pp. 163–175, Jan. 2016.
[8] J. Liu, N. Kato, J. Ma, and N. Kadowaki, "Device-to-device communication in LTE-advanced networks: A survey," *IEEE Commun. Surveys Tuts.*, vol. 17, no. 4, pp. 1923–1940, Nov. 2015.
[9] H. Peng *et al.*, "Performance analysis of IEEE 802.11p DCF for multiplatooning communications with autonomous vehicles," *IEEE Trans. Veh. Technol.*, vol. 66, no. 3, pp. 2485–2498, Mar. 2017.
[10] W. Fan, P. Kyösti, J. Ødum Nielsen, and G. Frølund Pedersen, "Wideband MIMO channel capacity analysis in multiprobe anechoic chamber setups," *IEEE Trans. Veh. Technol.*, vol. 65, no. 5, pp. 2861–2871, May 2016.
[11] *Test Plan for Mobile Station Over the Air Performance, Revision 3.3.5*, CTIA, Washington, DC, USA, Jul. 2016.
[12] W. Sun and J. Liu, "Coordinated multipoint based uplink transmission in internet of things powered by energy harvesting," *IEEE Internet Things J.*, vol. 5, no. 4, pp. 2585–2595, Aug. 2018.
[13] Y. Qi, P. Jarmuszewski, Q. Zhou, M. Certain, and J. Chen, "An efficient TIS measurement technique based on RSSI for wireless mobile stations," *IEEE Trans. Instrum. Meas.*, vol. 59, no. 9, pp. 2414–2419, Sep. 2010.
[14] W. Sun, J. Liu, and H. Zhang, "When smart wearables meet intelligent vehicles: Challenges and future directions," *IEEE Wireless Commun. Mag.*, vol. 24, no. 3, pp. 58–65, Jun. 2017.
[15] P. Shen, Y. Qi, W. Yu, and F. Li, "Inverse matrix auto-search technique for the RTS MIMO OTA test—Part 1: Theory," *IEEE Trans. Electromagn. Compat.*, vol. 59, no. 6, pp. 1716–1723, Dec. 2017.
[16] 3GPP, 2017. [Online]. Available: http://www.3gpp.org
[17] CTIA, 2017. [Online]. Available: http://www.ctia.org
[18] P. Shen, Y. Qi, W. Yu, and F. Li, "Eliminating RSARP reporting errors in the RTS method for MIMO OTA test," *IEEE Trans. Electromagn. Compat.*, vol. 59, no. 6, pp. 1708–1715, Dec. 2017.
[19] P. Shen, Y. Qi, W. Yu, F. Li, and J. Fan, "Fast and accurate TIS testing method for wireless user equipment with RSS reporting," *IEEE Trans. Electromagn. Compat.*, vol. 58, no. 3, pp. 887–895, Jun. 2016.
[20] J. Liu, S. Zhang, W. Sun, and Y. Shi, "In-vehicle network attacks and countermeasures: Challenges and future directions," *IEEE Netw. Mag.*, vol. 31, no. 5, pp. 50–58, Sep./Oct. 2017.
[21] P. Shen, Y. Qi, W. Yu, F. Li, and J. Fan, "Fast method for OTA performance testing of transmit–receive cofrequency mobile terminal," *IEEE Trans. Electromagn. Compat.*, vol. 58, no. 4, pp. 1367–1374, Aug. 2016.
[22] Y. Wang, S. Jin, S. Penugonda, and J. Fan, "Variability analysis of crosstalk among differential vias using polynomial-chaos and response surface methods," *IEEE Trans. Electromagn. Compat.*, vol. 59, no. 4, pp. 1368–1378, Aug. 2017.
[23] J. Dai, J. Liu, Y. Shi, S. Zhang, and J. Ma, "Analytical modeling of resource allocation in D2D overlaying multi-hop multi-channel uplink cellular networks," *IEEE Trans. Veh. Technol.*, vol. 66, no. 8, pp. 6633–6644, Aug. 2017, doi: 10.1109/TVT.2017.2675451.
[24] Y. Qi, P. Jarmuszewski, Q. Zhou, M. Certain, and J. Chen, "An efficient TIS measurement technique based on RSSI for wireless mobile stations," *IEEE Trans. Instrum. Meas.*, vol. 59, no. 9, pp. 2414–2419, Sep. 2010.

[25] Z. Liu, Y. Qi, F. Li, W. Yu, and J. Fan, "Fast band-sweep total isotropic sensitivity measurement," *IEEE Trans. Electromagn. Compat.*, vol. 58, no. 4, pp. 1244–1251, Aug. 2016.
[26] J. Liu, Y. Kawamoto, H. Nishiyama, N. Kato, and N. Kadowaki, "Device-to-device communications achieve efficient load balancing in LTE-advanced networks," *IEEE Wireless Commun. Mag.*, vol. 21, no. 2, pp. 57–65, Apr. 2014.
[27] Y. Qi and W. Yu, "Unified antenna temperature," *IEEE Trans. Electromagn. Compat.*, vol. 58, no. 5, pp. 1425–1431, Jun. 2016.
[28] Y. Qi *et al.*, "Objective total isotropic sensitivity measurement," *IEEE Trans. Electromagn. Compat.*, vol. 59, no. 6, pp. 1671–1676, Dec. 2017.
[29] General Test Systems Inc., 2018. [Online]. Available: http://www.generaltest.com/

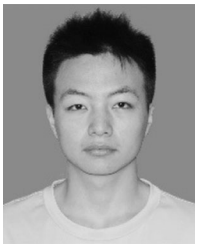

Penghui Shen (S'15) received the B.S. and M.S. degrees in electronic information and technology in 2013 and 2016, respectively, from Hunan University, Changsha, China, where he is currently working toward the Ph.D. degree in electronics. His research interests include single-input single-output and multi-input multi-output measurements for wireless devices, electromagnetic compatibility, and antenna design.

Yihong Qi (M'92–SM'11) received the B.S. degree in electronics from the National University of Defense Technologies, Changsha, China, in 1982, the M.S. degree in electronics from the Chinese Academy of Space Technology, Beijing, China, in 1985, and the Ph.D. degree in electronics from Xidian University, Xi'an, China, in 1989. From 1989 to 1993, he was a Postdoctoral Fellow and then an Associate Professor with Southeast University, Nanjing, China. From 1993 to 1995, he was a Postdoctoral Researcher with McMaster University, Hamilton, ON, Canada. From 1995 to 2010, he was with Research in Motion (Blackberry), Waterloo, ON, where he was the Director of Advanced Electromagnetic Research. He is currently the President and Chief Scientist with General Test Systems, Inc., Shenzhen, China. He founded DBJay in 2011, and he is the CTO of ENICE. He is also an Adjunct Professor with the Electromagnetic Compatibility (EMC) Laboratory, Missouri University of Science and Technology, Rolla, MO, USA, and an Adjunct Professor with Hunan University, Changsha, China. He is an inventor of more than 251 published and pending patents. He was a Distinguished Lecturer of the IEEE EMC Society for 2014 and 2015. He is the Chairman of the IEEE EMC TC-12. He received an IEEE EMC Society Technical Achievement Award in August 2017.

Wei Yu (M'13) received the B.S. degree in electrical engineering from Xi'an Jiaotong University, Xi'an, China, in 1991, the M.S. degree in electrical engineering from the China Academy of Space Technology, Beijing, China, in 1994, and the Ph.D. degree in electrical engineering from Xidian University, Xi'an, China, in 2000. From 2001 to 2003, he was a Postdoctoral Fellow with the University of Waterloo, Waterloo, ON, Canada. He was a CTO with Sunway Communications Ltd., from 2008 to 2012. He founded Antenovation Electronics Inc. in 2004 and cofounded General Test Systems Inc., Shenzhen, China, in 2012. He is a COO with DBJ Technologies, Zhuhai, China. He is an inventor of 91 published and pending patents. His current research interests include signal processing and mobile device test systems.

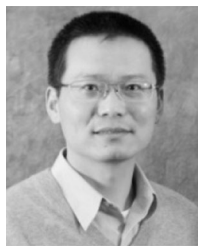

Jun Fan (S'97–M'00–SM'06–F'16) received the B.S. and M.S. degrees in electrical engineering from Tsinghua University, Beijing, China, in 1994 and 1997, respectively, and the Ph.D. degree in electrical engineering from the University of Missouri–Rolla, Rolla, MO, USA, in 2000. From 2000 to 2007, he was a Consultant Engineer with NCR Corporation, San Diego, CA, USA. In July 2007, he joined the Missouri University of Science and Technology (formerly University of Missouri–Rolla), where he is currently an Associate Professor with the Missouri S&T Electromagnetic Compatibility (EMC) Laboratory. His current research interests include signal integrity and electromagnetic interference (EMI) designs in high-speed digital systems, dc power-bus modeling, intersystem EMI and radio frequency interference, printed circuit board noise reduction, differential signaling, and cable/connector designs. He was the Chair of the IEEE EMC Society TC-9 Computational Electromagnetics Committee from 2006 to 2008 and was a Distinguished Lecturer of the IEEE EMC Society in 2007 and 2008. He is currently the Vice Chair of the Technical Advisory Committee of the IEEE EMC Society. He is an Associate Editor for the IEEE TRANSACTIONS ON ELECTROMAGNETIC COMPATIBILITY and the EMC MAGAZINE. He received an IEEE EMC Society Technical Achievement Award in August 2009.

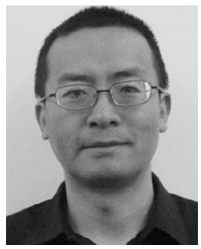

Zhiping Yang (S'97–M'00–SM'04) received the B.S. and M.S. degrees in from Tsinghua University, Beijing, China, in 1994 and 1997, respectively, and the Ph.D. degree from the University of Missouri–Rolla, Rolla, MO, USA, in 2000, all in electrical engineering. From 2000 to 2005, he was a Technical Leader with Cisco Systems, San Jose, CA, USA. From 2005 to 2006, he was a Principal Engineer with Apple Computer, Cupertino, CA. From 2006 to 2012, he was a Principal Engineer with Nuova Systems (which was acquired by Cisco in 2008) and Cisco Systems, San Jose. From 2012 to 2015, he was a Senior Manager with Apple, Cupertino. He is currently a Senior Hardware Manager with the Google Consumer Hardware Group, Google, Mountain View, CA, USA. He has authored or coauthored more than 40 research papers and 17 patents. His research interests include signal integrity and power integrity methodology development for die/package/board codesign, high-speed optical modules, various high-speed cabling solutions, high-speed DRAM/storage technology, high-speed serial signaling technology, and radio frequency interference. His research and patents have been applied in Google Chromebook, Apple iPhone 5S/6/6S, Cisco UCS, Cisco Nexus 6K/4K/3K, and Cisco Cat6K products. He received the 2016 IEEE EMCS Technical Achievement Award.

Songping Wu (S'08–M'11) received the B.S. degree from Wuhan University, Wuhan, China, in 2003, the M.S. degree from the Huazhong University of Science and Technology, Wuhan, China, in 2006, and the Ph.D. degree in electrical engineering from the Missouri University of Science and Technology, Rolla, MO, USA, in 2011. From 2011 to 2012, he was a Hardware Engineer with Cisco Systems, San Jose, CA, USA. From 2012 to 2016, he was a Senior Signal Integrity Engineer with Apple, Cupertino, CA. He is currently a De-Sense/SI Engineer with the Google Consumer Hardware Group, Google, Mountain View, CA. His research interests include in-device de-sense and co-existence in consumer hardware systems, as well as signal integrity and power integrity issues in package and high-speed printed circuit boards for digital devices and systems and application of signal integrity in sensors. He was the recipient of the IEEE Electromagnetic Compatibility Society President's Memorial Award in 2011.